Biochimica et Biophysica Acta 1861 (2017) 86–96

Contents lists available at ScienceDirect

Biochimica et Biophysica Acta

journal homepage: www.elsevier.com/locate/bbagen

Interdomain interactions rearrangements control the reaction steps of a thermostable DNA alkyltransferase

Castrese Morrone [a,1], Riccardo Miggiano [b,1], Mario Serpe [a], Alberto Massarotti [b], Anna Valenti [a], Giovanni del Monaco [a], Mosè Rossi [a], Franca Rossi [b], Menico Rizzi [b], Giuseppe Perugino [a,*], Maria Ciaramella [a,*]

[a] Institute of Biosciences and BioResources, National Research Council of Italy, Via P. Castellino 111, 80125 Naples, Italy
[b] DiSF-Dipartimento di Scienze del Farmaco, University of Piemonte Orientale 'A. Avogadro', Via Bovio 6, 28100 Novara, Italy

ARTICLE INFO

Article history:
Received 1 August 2016
Received in revised form 7 October 2016
Accepted 20 October 2016
Available online 22 October 2016

Keywords:
Alkylation damage
DNA repair
Fluorescent-based assay
Crystal structure
Conformational changes

ABSTRACT

Background: Alkylated DNA-protein alkyltransferases (AGTs) are conserved proteins that repair alkylation damage in DNA by using a single-step mechanism leading to irreversible alkylation of the catalytic cysteine in the active site. Trans-alkylation induces inactivation and destabilization of the protein, both *in vitro* and *in vivo*, likely triggering conformational changes. A complete picture of structural rearrangements occurring during the reaction cycle is missing, despite considerable interest raised by the peculiarity of AGT reaction, and the contribution of a functional AGT in limiting the efficacy of chemotherapy with alkylating drugs.
Methods: As a model for AGTs we have used a thermostable ortholog from the archaeon *Sulfolobus solfataricus* (*Ss*OGT), performing biochemical, structural, molecular dynamics and *in silico* analysis of ligand-free, DNA-bound and mutated versions of the protein.
Results: Conformational changes occurring during lesion recognition and after the reaction, allowed us to identify a novel interaction network contributing to *Ss*OGT stability, which is perturbed when a bulky adduct between the catalytic cysteine and the alkyl group is formed, a mandatory step toward the permanent protein alkylation.
Conclusions: Our data highlighted conformational changes and perturbation of intramolecular interaction occurring during lesion recognition and catalysis, confirming our previous hypothesis that coordination between the N- and C-terminal domains of *Ss*OGT is important for protein activity and stability.
General significance: A general model of structural rearrangements occurring during the reaction cycle of AGTs is proposed. If confirmed, this model might be a starting point to design strategies to modulate AGT activity in therapeutic settings.

1. Introduction

Alkylated-DNA protein alkyltransferases (called AGT, OGT, or MGMT, EC: 2.1.1.63) are specialized proteins that perform the direct repair of alkylation damage in DNA, mainly acting at position O^6 of guanines. They use a peculiar one-step mechanism, in which a single trans-alkylation reaction catalyses the transfer of the alkyl group from DNA to a cysteine residue in the protein active site, restoring the correct DNA structure with no need for other factors or energy source [1,2].

AGTs are evolutionary highly conserved, and orthologs from humans, bacteria and archaea have been extensively studied [2,3]. In particular, the human protein (hAGT) has raised considerable interest because its activity antagonizes the effect of alkylating drugs widely used in chemotherapy, and its overexpression is frequently associated with resistance to such drugs [2]. Moreover, certain AGT variants have been associated with the virulence of *Mycobacterium tuberculosis* species [4,5].

Previous structural and biochemical studies elucidated details of DNA binding, lesion recognition and repair by AGTs [4–13]. Invariably, the protein architecture consists of a highly conserved C-terminal (C_{ter}) domain, containing both the DNA binding helix-turn-helix motif and the catalytic site; and a N-terminal (N_{ter}) domain, whose function is less understood and has been suggested to assist the correct folding/stability of the C_{ter} domain [14] and contribute to optimal catalysis [4,5]. Upon lesion recognition, the alkylated base is flipped out from the regular base stacking of the double helix, and inserted into the protein active site, allowing the transfer of the alkyl moiety to the catalytic cysteine. The drawback of this elegant reaction is that once alkylated, the protein is irreversibly inactivated and destabilized, both *in vitro*

Abbreviations: BG-VG, SNAP-Vista Green™ substrate; C_{ter}, C-terminal domain; DDMP, Difference Distance Matrix Plot; dsDNA^m, O^6-methyl-guanine-containing double-strand DNA; DSF, Differential Scanning Fluorimetry; hAGT, human AGT; MD, molecular dynamics; N_{ter}, N-terminal domain; O^6-BG, O^6-benzyl-guanine; O^6-MG, O^6-methyl-guanine; RMSD, root-mean-square deviation; *Ss*OGT, *S. solfataricus* O^6-alkyl-guanine-DNA-alkyltransferase; *Ss*OGT^m, methylated *Ss*OGT.

* Corresponding authors.
E-mail addresses: giuseppe.perugino@ibbr.cnr.it (G. Perugino), maria.ciaramella@ibbr.cnr.it (M. Ciaramella).

[1] These authors contributed equally to the paper as First Authors.

http://dx.doi.org/10.1016/j.bbagen.2016.10.020
0304-4165/

and *in vivo* [15,16]. In human and yeast cells, the degradation of hAGT occurs through the ubiquitin-proteasome pathway [16] and might also affect other DNA repair pathways [17].

The molecular mechanisms underlying the AGT unfolding and degradation, which follow the alkylation of the active site cysteine, are only partially understood: conformational changes and modification of intramolecular interactions are likely to be associated to each step of the reaction cycle. Evidence of some changes occurring after hAGT methylation has been provided [18–20]; however, the intrinsic instability of alkylated AGTs has been an important limitation to structural and biochemical studies [19].

These limitations have been overcome by the availability of a thermostable DNA alkyl-transferase from the archaeon *Sulfolobus solfataricus* (*Ss*OGT) [11], which proved to be a convenient model for AGTs. In this hyperthermophilic microorganism, alkylating agents action is potentiated by the high temperature of growth, resulting in an apoptotic-like effect, characterized by DNA fragmentation and degradation of key proteins involved in genome stability [3,21–24]. *Ss*OGT is also degraded after treatment with lethal doses of alkylating agents, thus recalling its fate in human cells [11]. Although alkylation reduces the exceptional stability of *Ss*OGT *in vitro*, the alkylated protein is stable enough to allow structural and biochemical analysis at operational temperatures [10,11]. We exploited this unique property to obtain direct structural and biochemical information on *Ss*OGT in its free, DNA-bound and methylated post-reaction form [10]. Importantly, in contrast to the 3D structure of the methylated hAGT (obtained by soaking protein crystals in substrate solutions; [19]), the 3D structure of *Ss*OGT was obtained by crystallizing the protein previously methylated in solution and purified, which might better reflect the physiological conformation of the alkylated protein, allowing free movements that could otherwise be restricted in crystals.

The available *Ss*OGT structures are useful tools as they open the possibility of understanding how alkylation triggers the protein unfolding and describing the conformational changes associated to each step of the reaction. So far, this analysis showed significant changes occurring upon *Ss*OGT active site cysteine (C119) methylation in discrete regions of the protein and allowed the identification of one interaction whose methylation-induced perturbation leads to protein destabilization [10] (see also below).

In this paper we report a further step forward, as we analyse the conformational changes and intramolecular interactions, which are perturbed during binding of *Ss*OGT to methylated DNA, before the transmethylation reaction is completed. Moreover, we solved the crystal structure of the *Ss*OGT-C119F mutant, gaining an indirect insight into the possible conformation adopted by the protein upon the removal of an aromatic and bulky adduct from the DNA. Taken as a whole, the structural, biochemical and molecular dynamics studies of ligand-free, methylated and mutated forms of *Ss*OGT suggested a model for the alkylation-induced unfolding and degradation of this protein, which is of possible relevance also for other AGTs.

2. Materials and methods

2.1. Reagents

All chemicals were from Sigma, and synthetic oligonucleotides were from EuroFins (Milan, Italy). *E. coli* ABLE C and JM109 strains, as well as *Pfu* DNA polymerase were purchased from Stratagene (La Jolla, CA). The SNAP-Vista Green™ substrate (BG-VG) was from New England Biolabs (Ipswich, MA), and SYPRO Orange™ was from Thermo Fisher Scientific (NYSE, TMO).

2.2. DNA site-directed mutagenesis and protein production

Starting from the *S. solfataricus ogt* gene cloned in the pQE31™ vector [11] used as template, mutants were obtained by applying the GeneTailor™ Site-Directed Mutagenesis System (Invitrogen) method, by using oligonucleotide pairs listed in the Supplementary Table S1. All proteins were heterologously expressed in the *E. coli* ABLE-C or JM109 strain and purified by affinity chromatography and desalting steps, as described [11].

2.3. Determination of the catalytic activity by fluorescent assay

The catalytic activity was measured by using a fluorescent assay we previously set up and validated, based on the use of derivatives of O^6-benzyl-guanine (O^6-BG), which is known to inhibit AGTs by covalent transfer of the benzylic group to the active site cysteine. Our assay employs a fluorescein-conjugated derivative of O^6-BG (SNAP-Vista Green™, hereafter called BG-VG), which labels the protein covalently and stoichiometrically [4,5,10,11,25]. For the catalytic constants determination, fixed *Ss*OGT and BG-VG concentrations were incubated for different time spans; the fluorescence intensity of the labelled protein band in SDS-PAGE was quantified and used to calculate second-order rate constants [11,26].

2.4. Determination of the DNA repair activity by the IC_{50} method

The efficiency of repair of AGTs depends on their ability to bind DNA, recognize the lesion and repair it: all these functions have been analysed by a unique competition assay according to the IC_{50} method, where a dsDNA oligonucleotide containing a single O^6-MG was used as a competitor in the reaction of *Ss*OGT with BG-VG. Finally, K_{DNA} constants were calculated from the obtained IC_{50} values [10,27].

2.5. Differential Scanning Fluorimetry (DSF) assay for the protein stability determination

The stability against thermal denaturation was followed spectrofluorimetrically as described [10], adapting the method proposed by the group of Vedadi [28]. Because of the intrinsically high stability of *Ss*OGT, thermal stability scans from 25.0 to 95.0 °C were performed at a scan rate of 0.2 °C min^{-1} (5 min per cycle with an increase of 1.0 °C per cycle). Normalized data of the fluorescence intensities *vs* temperature from three independent experiments were fitted with the Boltzmann equation [10,28] allowing the determination of the T_m values.

2.6. Crystallization and data collection

The purified *Ss*OGT-C119F mutated variant was subjected to robot-assisted crystallization trials (Oryx4; Douglas Instruments) using commercial screens from Hampton Research (Crystal Screen, Crystal Screen II, PegIon and PegIon II) and Qiagen (Classics Suite and Classics Suite II), applying the vapor diffusion method in sitting drop. Protein crystals, in the form of thin needles, grew to their maximum dimensions in three weeks at 4 °C in drops obtained by mixing 0.5 μL of a 5.3 mg mL^{-1} protein solution and an equal volume of a precipitant solution containing 0.2 M ammonium phosphate monobasic and 20.0% W/V PEG 3350. The single crystals were cryo-protected in precipitant solution containing 15.0% glycerol, mounted in cryo-loop, and flash-frozen in liquid nitrogen at 100 K for subsequent X-ray diffraction analysis. Diffraction datasets were collected at the ID29 beamline at the European Synchrotron Radiation Facility (ESRF, Grenoble, France) equipped with a Pilatus 6M-F, at a wavelength of 1.008 Å. A data collection was performed up to 2.7 Å of resolution and the complete dataset was indexed with IMOSFLM program [29], allowing to assign the crystal to the orthorhombic space group *P*212121, with cell dimensions a = 52.86 Å b = 85.85 Å c = 98.46 Å, containing two molecules per asymmetric unit, with a Matthews coefficient and a solvent content of 2.94 $Å^3$ Da^{-1} and 58.19%, respectively. Further data analyses were carried out using the CCP4 suite programs COMBAT and SCALA [30].

2.7. Structure determination, model building and refinement

The initial phases for solving the structure of the *Ss*OGT-C119F variant were generated by molecular replacement with the program PHASER [31] of the PHENIX software suite [32,33], using the structure of *Sulfolobus solfataricus* wild type OGT (PDB ID: 4ZYE) as the search model. In this structure, the catalytic cysteine at position 119, the water and the ligand molecules have been omitted. Model building was performed with the program COOT [34] and crystallographic refinement was carried out with PHENIX [32]. Data converged to the R_{factor} and R_{free} values of 0.172 and 0.237, respectively, with good geometry.

2.8. Protein structure accession numbers

The atomic coordinates and structure factors of the *Ss*OGT-C119F mutated variant have been deposited in the Protein Data Bank (http://www.rcsb.org) under the accession code ID: 5LLQ.

2.9. Molecular dynamics (MD)

Crystallographic structure of ligand-free *Ss*OGT (PDB ID: 4ZYE) and its mutants C119A (PDB ID: 4ZYD), C119L (PDB ID: 4ZYH) and C119F (PDB ID: 5LLQ) were used for the initial coordinates of the MD simulations. MD simulations were performed using GROMACS 5.1 software [10.1016/j.softx.2015.06.001] with the GROMOS 54a7 force field [10.1007/s00249-011-0700-9] implemented in Intel Xeon Octa Core processor with Linux environment. In our models, basic residues are protonated and acidic residues are unprotonated. Systems were neutralized and solvated in a periodic octahedric box containing a simple point charge (SPC) water model [31]. Two series of simulations were carried out: at a constant temperature of 353 K since *Ss*OGT is a hyperthermophile enzyme, and at a constant temperature of 500 K to analyse the protein unfolding. Before every MD simulation, the internal constraints were relaxed by energy minimization, followed by equilibration (100 ps at constant temperature and 100 ps at constant pressure) under position restraints of the carbon backbone atoms. During the MD runs, covalent bonds in the protein were constrained using the LINCS algorithm [10.1002/(SICI)1096-987X(199709)18:12<1463::AID-JCC4>3.0.CO;2-H]. The SETTLE algorithm was used to constrain the geometry of water molecules [10.1002/jcc.540130805]. Berendsen's coupling algorithm was used to maintain the simulation under constant pressure and temperature [10.1063/1.448118]. Van der Waals forces were treated using a cutoff of 1.0 nm. Longrange electrostatic forces (r.1.0 nm) were treated using particle mesh implemented in the Verlet method [10.1103/PhysRev.159.98]. Through the production runs, the trajectory data were saved every 1 ps, and the total duration of the simulations was 200 ns.

Root-mean-square deviations (RMSD) were calculated taking the energy-minimized structure as a reference (Supplementary Fig. S1). Principal components analysis (PCA) of the protein motion was determined from the diagonalization of the covariance matrix of the interatomic fluctuation [10.1002/prot.340170408]. Average conformations were calculated from the variance-covariance matrix of all protein atoms during the equilibrium time of the run. Tools from the GROMACS package were used for the analysis of the data.

2.10. Data analysis

Prism Software Package (GraphPad Software) and GraFit 5.0 Data Analysis Software (Erithacus Software) were used for corrected data fitting using appropriate equations.

Difference Distance Matrix Plots (DDMPs) were obtained by using the CMView v1.1.1 freeware. All the structures used in this analysis (free *Ss*OGT; *Ss*OGT-C119A mutant bound to DNA; methylated *Ss*OGT) were aligned by the computation of Needleman-Wunsch sequence method, and choosing all types of amino acid contacts with a cut-off of 8.0 Å.

All the figures illustrating structural analysis were generated by Pymol freeware version 1.7 (Schrodinger, LLC., http://www.pymol.org) using standard code for amino acid atoms colouring.

3. Results and discussion

3.1. SsOGT conformational modifications associated with O^6-MG recognition and binding

In order to describe the complete picture of conformational changes occurring throughout the DNA repair reaction, we performed unbiased DDMP analysis, by comparing the network of intramolecular interactions observed in the available 3D structures of *Ss*OGT. A preliminary analysis previously performed on ligand-free *vs* *Ss*OGT^m structures gave important hints on changes occurring upon protein methylation ([10]; see also below). We have now extended and further refined this analysis by comparing the free, DNA-bound and methylated *Ss*OGT (*Ss*OGT^m) structures, taking into account all intramolecular interactions, including those formed by the atoms of the protein backbone (Fig. 1).

The crystal structure of the *Ss*OGT inactive mutant, C119A, in complex with a methylated dsDNA^m oligonucleotide showed that substrate binding does not affect significantly the protein overall structure [10]; however, structural changes in specific protein regions are expected to occur, in order to accommodate the double helix as well as the methylated base, which adopts an extra-helical configuration in the complex. Indeed, the DDMP analysis comparing the free and DNA-bound protein forms showed an extensive reshaping of the molecule, with movements involving a number of residues and leading to a lot of lost and gained interactions when the protein contacts DNA and flips out the O^6-MG into its active site (Fig. 1a). The DDMP analysis comparing the DNA-bound and *Ss*OGT^m structures, which corresponds to the DNA-free protein in its post-reaction form, showed an almost symmetrical pattern, with most changes found in the DNA-bound structure no longer present (compare Fig. 1b and a); those changes, which correspond mainly to intra-domain interactions, are thus a consequence of the binding of the natural substrate, as expected from the induced fit model for a genuine enzyme.

However, like all AGTs, *Ss*OGT is not a true enzyme, and irreversible methylation has dramatic consequences on its structure [10]; consistently, DDMP analysis comparing the *Ss*OGT^m with the free and DNA-bound structures showed multiple modified contacts (Fig. 1c). We argued that interdomain interactions should have a major role in securing the overall protein stability, and could be reasonable candidates to trigger the protein destabilization; thus, we focused our attention on three clusters of interactions occurring at the interface between the N_{ter} and C_{ter} domains. Two such clusters were already identified in a previous analysis [10]: in particular, cluster 1 corresponds to perturbation of the interaction between the D27 residue in the N_{ter} domain and the R133 residue in the C_{ter} domain, due to a *ca.* 60° clockwise rotation of the latter (inset 1 in Fig. 1c; d); this modification leads to strong destabilization of the overall structure. The second cluster corresponds to a loss of interactions caused by the *ca.* 3.0 Å movement of the C-side of the conserved H2 helix away from the overall structure upon alkylation (Fig. 1c, inset 2; Fig. 1d). Both modifications were found in the methylated protein, but not in the DNA-bound protein, thus suggesting that they are a direct consequence of the active site alkylation (compare DDMPs in Fig. 1b and c).

In addition, our current analysis highlighted another region where conformational changes occur, in particular at the interface between the N_{ter} domain and the connecting loop (indicated in inset 3 of Fig. 1c; d) which, in contrast to clusters 1 and 2, is common to both DNA-bound and *Ss*OGT^m. This cluster is characterized by a number of lost interactions at the level of a complex network involving the E44,

K48, N59, R61 and E62 residues (hereafter called *K48-network*). In the free *Ss*OGT, these residues are close to each other (2.9 Å distance on average), consistent with an ionic/hydrogen bond network (Fig. 2 and Table 1). In both the DNA-bound and methylated forms of the protein, the E44 and K48 appear to flip out, moving away from the body of the protein (Fig. 2). The former loses its hydrogen-bond with the E62,

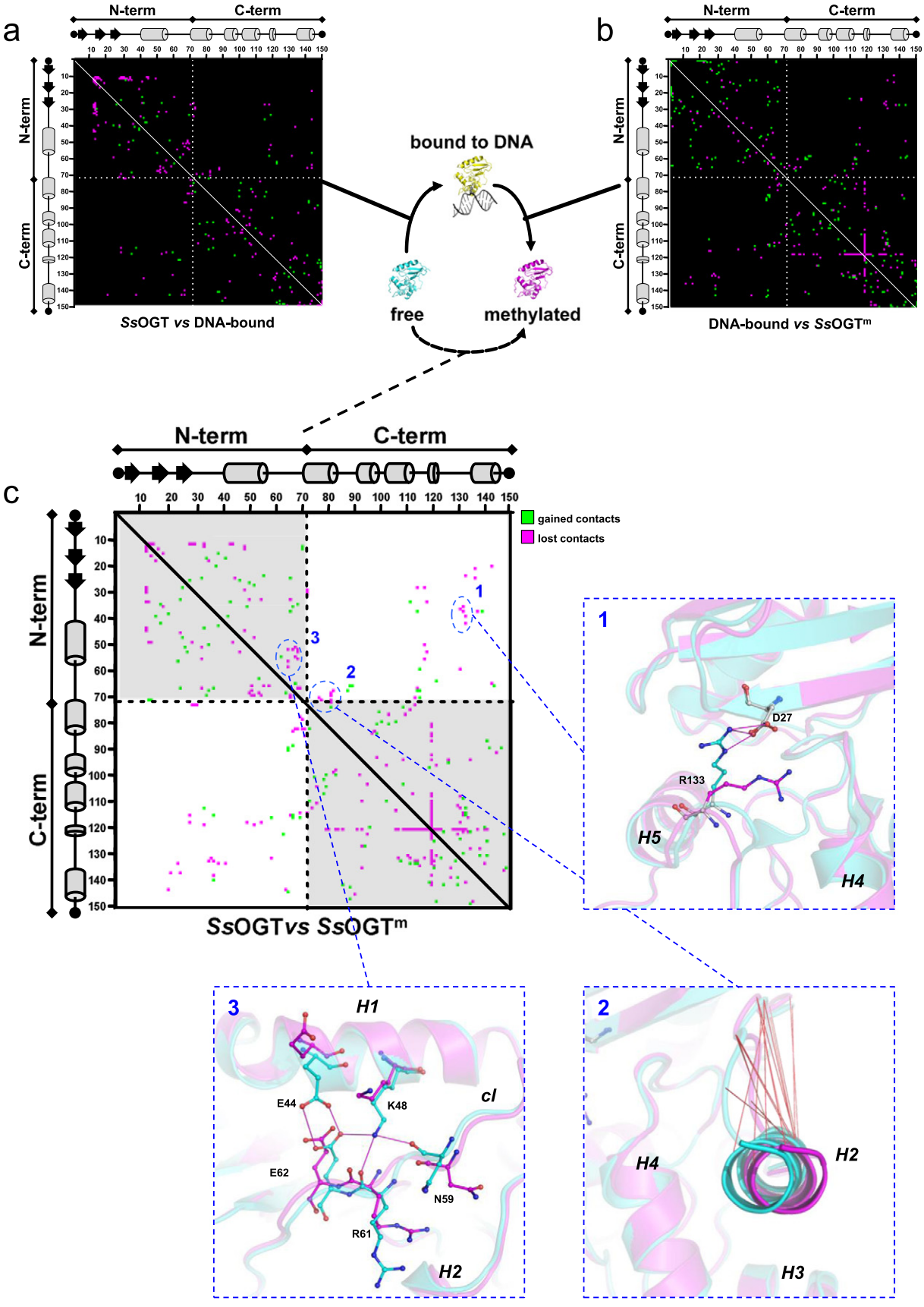

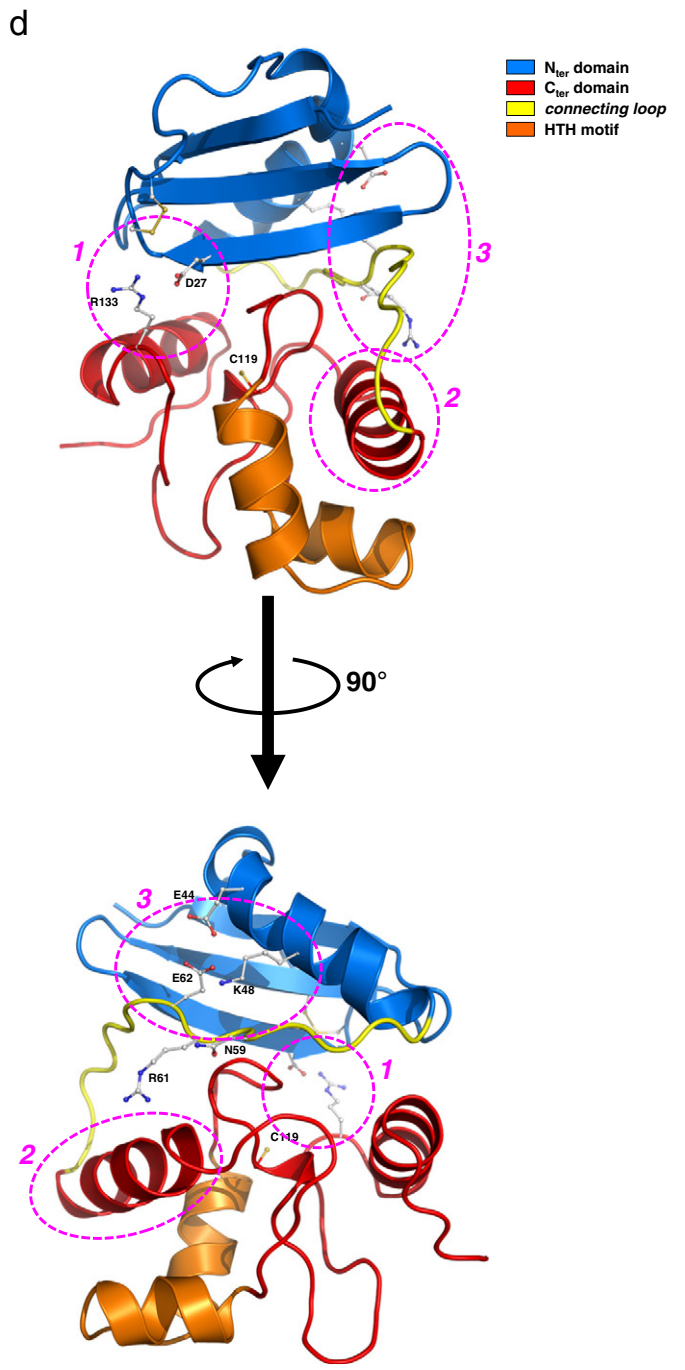

Fig. 1. The stages of the SsOGT activity analysed by DDMP. Available structures were compared in pairs, as indicated, leading to three distinct DDM plots (a, b and c). Clusters of lost (*in magenta*) and gained (*in green*) interactions were numbered and described in the text. Insets represent the position of the identified interactions of each corresponding cluster on the free protein 3D structure. *Ss*OGT, the DNA-bound and *Ss*OGT^{m} were represented *in cyan*, *yellow* and *magenta* colour, respectively. (d) Overall structure of the free *Ss*OGT, where identified clusters are numbered as in (c) and indicated in magenta. Amino acid atoms are coloured according the CPK convention (carbon, *in white or in the corresponding colour* of each 3D structure; oxygen, *in red*; nitrogen, *in blue*, sulphur, *in yellow*).

whereas the conformational change of the K48 residue has a stronger impact, perturbing its interactions with the N59, R61 and E62 (Fig. 2 and Table 1).

Taken together, these observations suggest that lesion recognition and alkylation trigger distinct modifications of intramolecular interactions in *Ss*OGT: whereas the changes at the level of cluster 1 and 2 occur only upon irreversible trans-alkylation of the catalytic cysteine, those observed in the *K48-network* might be a consequence of lesion recognition/steric hindrance of the active site, since they are already found in protein in complex with the methylated DNA and are retained in the post-repair protein structure devoid of DNA. Importantly, all three clusters occur at the interface between the two domains, suggesting that the interdomain communication plays important role in multiple steps of the reaction.

3.2. Structural analysis of the SsOGT-C119F mutated variant

To confirm the hypothesis that the observed rearrangements of the *K48-network* are linked to the presence of chemical groups in the active site, we analysed the configuration of this network in the C119L mutant (PDB ID: 4ZYH), in which a leucine residue replaces the catalytic cysteine [10]. This mutant showed biochemical and structural features consistent with the hypothesis that the L119 residue mimics an "isopropylation" of the active site [10]. Similarly to what has been observed in the crystal structure of the DNA-bound and *Ss*OGT^{m}, in the C119L mutant structure a displacement of the E44 residue was observed (Fig. 2); however, most distances among residues in the *K48-network* were not significantly affected (Fig. 2 and Table 1). The reasons for the difference with respect to the *Ss*OGT^{m} structure are currently not clear. We previously observed that the C119L protein 3D structure does not completely overlap the *Ss*OGT^{m} structure [10], suggesting that the C119L mutant might not be an optimal model of *Ss*OGT alkylation. Therefore, we sought to obtain independent experimental support to our hypothesis.

We previously obtained the C119F mutant that, by virtue of the presence of a phenylalanine residue substituting the catalytic cysteine in the active site, mimics a "benzylated" form of the protein. Consistently, biochemical analysis showed that, similarly to the C119L mutant, this protein is also greatly destabilized, and preliminary crystallization trials failed [10]. Similar results were obtained with the C145F mutant of hAGT, which was extremely unstable when heterologously expressed in *E. coli* [19]. Nevertheless, new crystallization trials were successful and allowed the resolution of the *Ss*OGT-C119F structure at 2.7 Å (Fig. 3 and Table 2). Interestingly, the structural analysis of *Ss*OGT-C119F revealed elements of novelty compared to the available AGT structures that represent the protein at the different stages of the alkyltransferase reaction [4,7–10,13,19,36–38]. It has been suggested that alkylation of the active site could trigger movements of the conserved recognition helix belonging to the HTH motif, explaining the *in vivo* destabilization of the reacted form of the protein. However, a comparative structural analysis performed on the ligand-free and alkylated forms of the human enzyme did not reveal significant shifts of the correspondent recognition helix away from the N_{ter} domain of the protein [18,19]. By analysing the *Ss*OGT-C119F structure, we directly observed for the first time a repositioning of the recognition helix H4, probably induced by the need to make room for the alkyl adduct in the active site pocket (*i.e.* the aromatic moiety of F119 side chain). Concomitantly, we observed a repositioning of the N111 of the highly conserved *Asn-hinge* of the protein (Fig. 3, inset), a residue that is crucial for protein stability; in fact, the mutation to alanine of the equivalent asparagine residue (N137) in the human ortholog resulted in a dramatic protein destabilization [35].

In this new conformation, N111 moves approximately 2.0 Å toward the active site loop that constitutes part of the opposite wall of the catalytic cavity, and establishes a hydrogen bond with the hydroxyl moiety of the S132 residue (Fig. 3). A partial movement of S132 was previously observed in the crystal structure of *Ss*OGT^{m} and was associated with the loss of interaction between R133 and D27, triggering protein unfolding [10]. Moreover, the structural analysis of *Ss*OGT-C119F confirms our hypothesis that alkylation of the active site induces further amino acid repositioning that alters the protein stability. Indeed, the peculiar arrangement of ionic bonds observed inside the *K48-network* of the ligand-free protein in the *Ss*OGT-C119F structure is destroyed at the

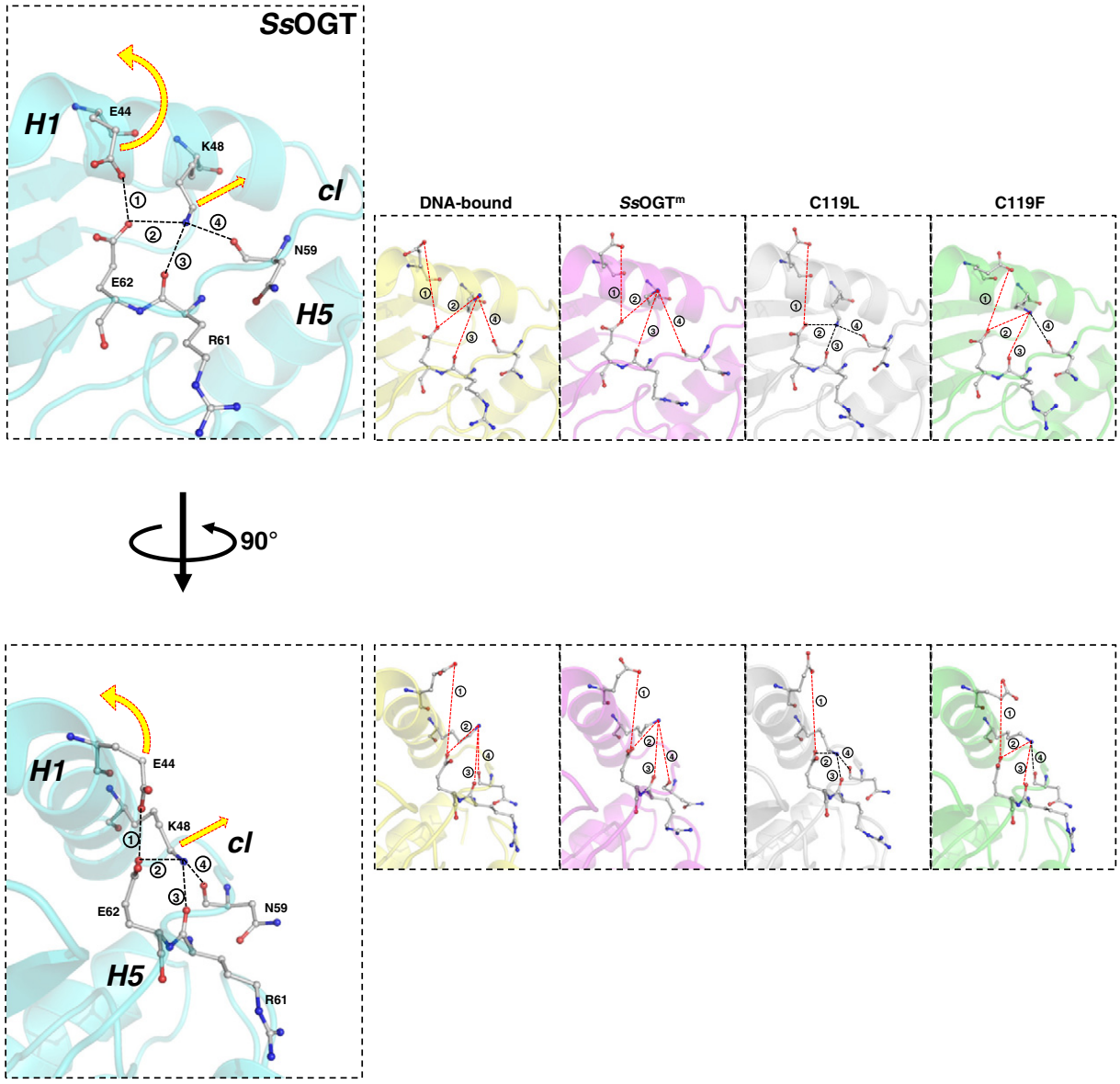

Fig. 2. The *K48-network* in SsOGT. 3D structures are in transparent *cartoon* representation, in a colour code as in Fig. 1. The *K48-network* residues are indicated and displayed in *ball and stick* format. Yellow arrows illustrate the movement of side chains on the structure, during the stages of the *Ss*OGT activity and in the cysteine 119 mutants (C119L *in grey*, C119F *in green*). H1, H5 and cl stand for Helix 1, Helix 5 and the connecting loop, respectively. Amino acid atoms are coloured as in Fig. 1.

same extent as in the methylated form of the protein (Fig. 2 and Table 1). The extent of the movements detected in the *K48-network* as a consequence of the active site modification is summarized in Table 1.

As previously demonstrated, transalkylated AGTs are permanently inactivated and prone to degradation both *in vivo* and *in vitro* [1,2,10–12,19]. The opening of the tertiary structure that we observed in the *Ss*OGT-C119F mutant may represent the mechanism for protein destabilization and its consequent degradation *in vivo*. Overall, the analysis of the *Ss*OGT-C119F structure allowed us to better describe the conformational modifications that characterize the *Ss*OGT protein, following the entire alkyltransferase reaction.

The differences between the C119F and C119L structures at the level of the *K48-network* are currently difficult to interpret: for instance, although the interactions formed by the K48 residue were similar in the C119F and in the *Ss*OGT^{m}, but not in the C119L, the reverse was true for the position of the E44 residue (Table 1; Figs. 2 and 3), showing that neither mutant could faithfully recapitulate all conformational changes triggered by physiological alkylation. These results should suggest caution, in general, in the interpretation of structure-function data obtained with synthetic mutant proteins. Indeed, post-translational modifications of a native protein might affect the protein conformation in a different manner as compared with amino acid substitutions, which are incorporated in the protein structure co-translationally. In our case, the availability of structural and biochemical data obtained from two independent mutants, along with the physiologically methylated protein, helped to partially overcome these limitations.

Table 1
Comparison of the distances among the *K48-network* residues in all available *Ss*OGT 3D structures.

Entry[a]	Interaction	Distance (Å)				
		*Ss*OGT	DNA-bound	*Ss*OGT^{m}	C119L	C119F
①	E44 (Oε1) ⇔ E62 (Oε2)	2.63	8.74	7.50	8.11	6.57
②	K48 (N) ⇔ E62 (Oε2)	3.02	5.33	4.82	3.12	4.60
③	K48 (N) ⇔ R61 (Oα)	3.05	6.67	6.39	3.21	5.01
④	K48 (N) ⇔ N59 (Oα)	2.87	5.08	6.73	3.06	3.80

[a] The encircled numbers refer to the distances graphically represented in Fig. 2.

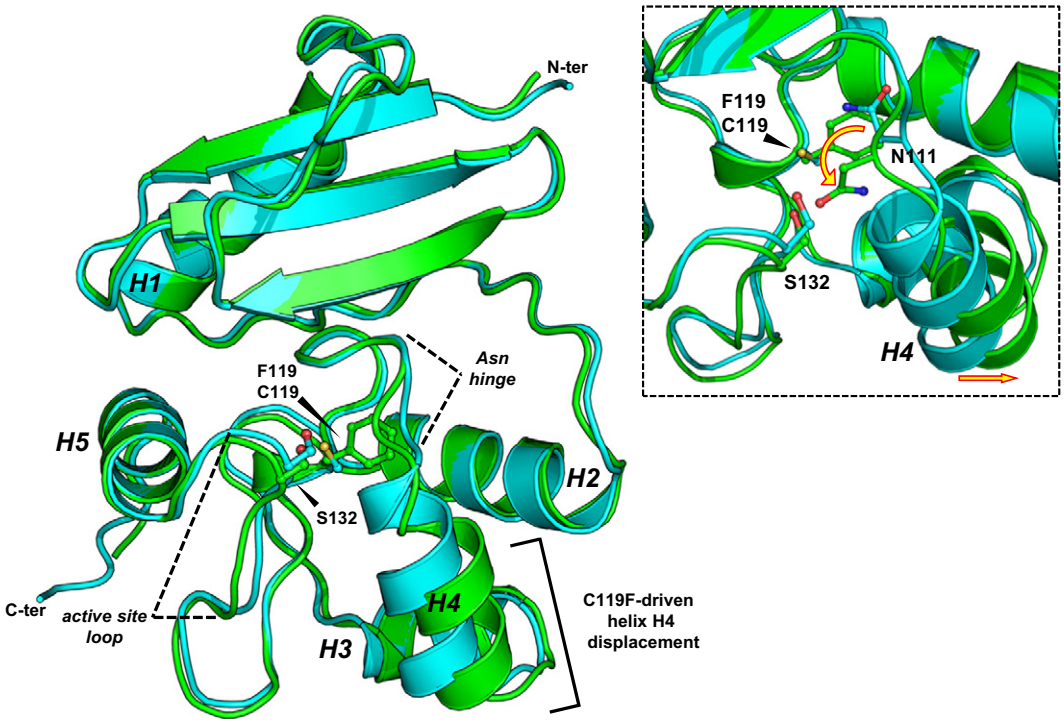

Fig. 3. Structural analysis of SsOGT-C119F. Cartoon representation of the crystal structure of the ligand-free form of wild-type *Ss*OGT (pdb: 4ZYE: *in cyan*) and of the C119F mutated variant (pdb: 5LLQ, *in green*), upon optimal superposition. A zoomed view of the conformational changes observed in the C119F variant active site appears in the inset on the right. The yellow arrows indicate the relevant movements of the N111 residue and of the recognition helix H4, as described in the main text. For the colour code of amino acid atoms, refer to the description in Fig. 1.

3.3. Molecular dynamics (MD) simulations

In order to obtain independent information on the role of *Ss*OGT residues in the protein stability, we followed the mobility of *Ss*OGT residues by MD simulations. *Ss*OGT wild type, C119A, C119L, and C119F mutants were simulated for 200 ns at 353 K (80.0 °C). To assess the simulation stability, some geometrical properties such as the average values of the radius of gyration (R_G), the number of intra-protein hydrogen bonds (HB_{intra}) and the solvent-accessible surface area (SASA), both apolar and polar, were monitored as a function of time; all these properties indicated that the structures were stable during the entire simulation (Table 3). Information about protein equilibration is provided by convergence of RMSD of the atomic position, with respect to the initial structure, calculated as function of time. The comparison of these values (Table 3) and the RMSD plots (Fig. S1b) indicated that free *Ss*OGT requires less time to equilibrate and its RMSD is the lowest. The resulting average conformation for each simulation was used to perform a second MD simulation for 200 ns at 500 K (227.0 °C, Supplementary Table 2). Thus, the MD simulation at 353 K was used to analyse the protein structure at physiological temperature, while the one at 500 K was used to interpret the effect of mutations on structural changes.

In order to obtain further insights into the dynamics of *Ss*OGT structure, the principal component analysis (PCA) was used to dissect out cooperative inner motions. In free *Ss*OGT (Fig. 4), at 353 K we observed movements of a few residues; at 500 K the internal molecular motion was obviously increased, especially in the C_{ter} domain, with significant movements of residues in helices H3, H4 and H5. By contrast, the N_{ter} domain showed higher stability, which can be explained in terms of rigid body-like behavior, since all its secondary structures moved together in the same direction, and the whole domain behaved like a single object. In the *Ss*OGT mutants (Fig. S1a), the motions in the MD simulations performed at 353 K showed that overall molecular internal motion increases: in particular, the *K48-network* region was more

Table 2
Data collection, phasing, and refinement statistics of the *Ss*OGT-C119F mutant.

Data collection	
Space group	*P*212121
Wavelength (Å)	1.008
Resolution (Å)	2.7
Total reflections	51,418
Unique reflections	12,411
Mean (I)/sd (I)	10.26 (3.35) [a]
Completeness (%)	96.5 (97.7) [a]
Multiplicity	4.1 (4.3) [a]
R_{merge} (%)	10.2
R_{meas} (%)	11.6
Refinement	
R_{factor}/R_{free} (%)	17.2/23.7
Protein atoms	2380
Ligand atoms	12
Water molecules	30
R.M.S.D. bonds (Å)	0.016
R.M.S.D. angles (°)	1.38
Average B (Å^2)	
Protein	32.40
Solvent	30.20
Ligands	47.40

Table 3
Selected structural properties of *Ss*OGT structures at 353 K.

System	R_G (nm)	HB_{intra}	Apolar SASA (nm^2)	Polar SASA (nm^2)	Cα RMSD (nm)	RMSD (nm)
*Ss*OGT	1.53 ± 0.02	100 ± 6	42 ± 2	50 ± 2	0.13 ± 0.03	0.23 ± 0.04
C119A	1.56 ± 0.01	101 ± 6	37 ± 1	54 ± 1	0.16 ± 0.04	0.52 ± 0.17
C119L	1.54 ± 0.02	96 ± 6	37 ± 2	53 ± 2	0.14 ± 0.03	0.39 ± 0.19
C119F	1.56 ± 0.02	97 ± 5	38 ± 2	54 ± 2	0.15 ± 0.03	0.39 ± 0.16

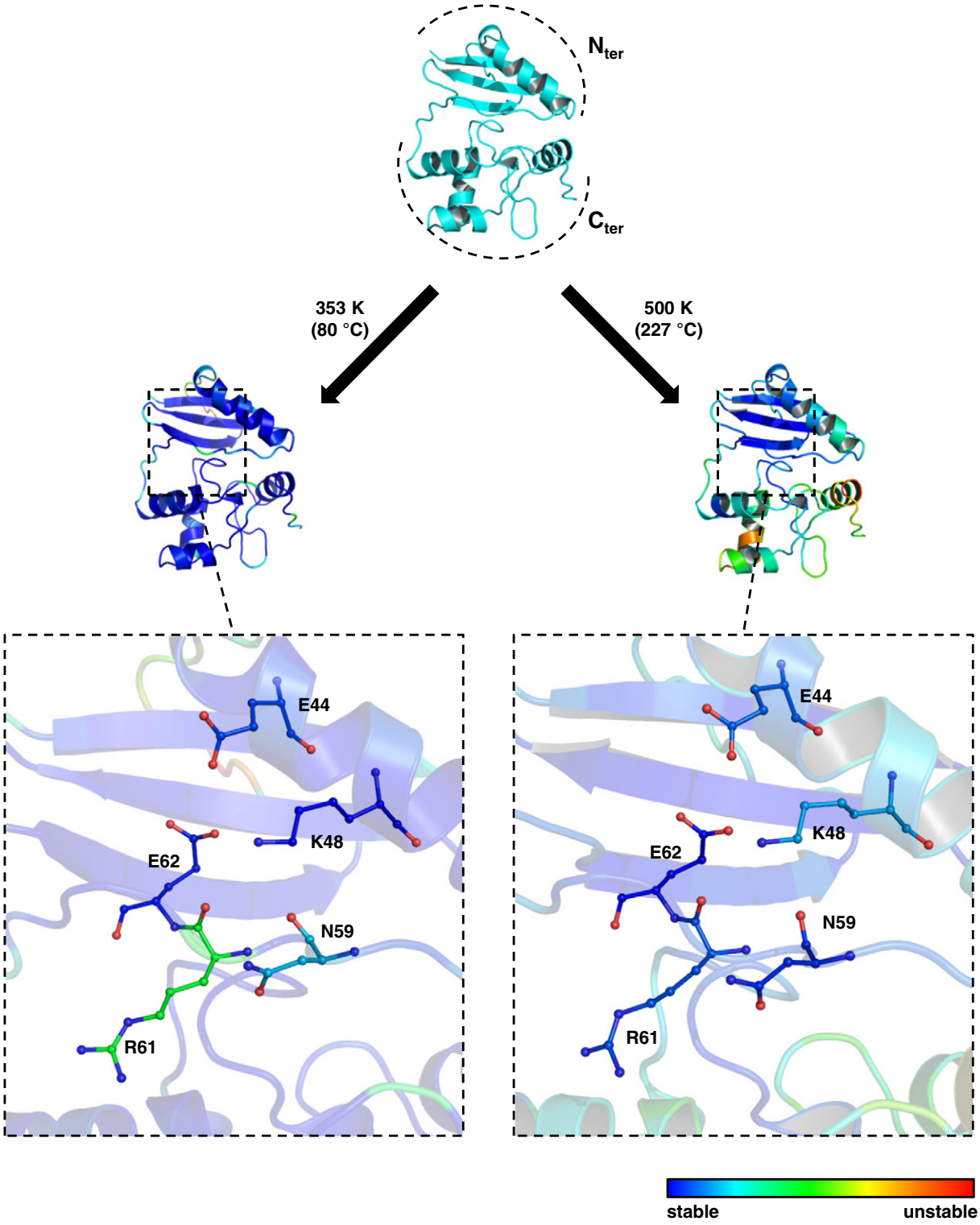

Fig. 4. PCA analysis of wild type SsOGT MD simulations. PCA analysis was performed to analyse the dynamics of residues during the MD simulations performed at 353 and 500 K. A colour scale is used to indicate the stable (*blue*) and unstable (*red*) portions of the protein structures. Detail of *K48-network* region of both MD simulation results is depicted. Amino acid atoms are coloured as described in Fig. 1.

unstable in all mutant structures, as compared with the wild-type. The dramatic effect of mutations on protein stability was even more evident in MD simulations at 500 K (Supplementary Table 2). The mutant structures showed overall larger movements than wild type *Ss*OGT: these movements were mainly in the C_{ter} domain of the protein, consistently with our previous analysis which identified in this domain nuclei of destabilization that could provide explanation of protein degradation *in vivo* upon alkyltransferase reaction, *i.e.* destroyed interactions and the displacement of conserved α-helixes (H2 and H4) [10]. In all mutants, strong movements were also observed in the N_{ter} domain, which cannot be considered as rigid-body in these structures.

The above analysis confirmed that *Ss*OGT stability depends on chemical modification of the catalytic cysteine, and all the mutations that mimic different adducts at the C119 residue have dramatic effects,

Table 4
Biochemical characterization of the activities and the stability of the *K48-network* mutants, in comparison with the wild type *Ss*OGT.

	Catalytic activity BG-VG (M^{-1} s^{-1})[a]	DNA repair activity K_{DNA} (μM)[b]	Thermal stability T_m (°C)[c]	Note
*Ss*OGT	2730 ± 320	0.83 ± 0.02	80.0 ± 0.4	From ref. [10]
E44L	1960 ± 410	0.66 ± 0.13	80.7 ± 0.1	This study
K48A	3090 ± 240	1.61 ± 0.30	72.0 ± 0.3	This study
K48L	2880 ± 330	1.59 ± 0.23	70.4 ± 0.3	This study

[a] Second-order rate constants of the trans-alkylation activity at 25.0 °C on the fluorescent substrate from three independent experiments, accordingly to the conditions previously reported [10] (see Materials and methods).
[b] Competition assay with BG-VG and a methylated-dsDNA oligonucleotide for 10 min at 50.0 °C. IC_{50} values were from three independent experiments; K_{DNA} values were obtained as shown in Materials and methods.
[c] Data obtained from three independent DSF experiments, as described in Materials and methods.

decreasing the overall protein stability and enhancing residue movements at high temperature. Increased movements were observed in the two protein domains, as well as at the level of the interdomain interface, where the D27-R133 and *K48-network* interactions are perturbed.

3.4. Analysis of the functional role of the K48-network

In order to establish the role of the *K48-network* in *Ss*OGT stability and activity, we prepared three site-directed mutants carrying substitutions of crucial residues in the network, namely E44L, K48A and K48L.

We analysed the catalytic and DNA repair activity of these mutants by using the fluorescence based assays previously developed [10,11]. The former was determined by measuring the efficiency of the alkyl-transfer reaction with the synthetic substrate BG-VG; at 25.0 °C, the catalytic activity of mutants was not significantly different from that of the wild-type protein (Table 4). DNA repair activity assays were performed by using a dsDNA^{m} as a competitor of the fluorescent substrate, thus giving a measure of the overall protein activity [10,11]. As shown in Table 4, whereas the efficiency of lesion repair by the E44L mutant was similar to that of the wild-type *Ss*OGT, both K48 mutants showed a slight reduction of the repair efficiency (K_{DNA} of 1.6 *vs* 0.8 μM at 50.0 °C).

In thermal stability assays, the E44L mutant showed the same resistance to thermal denaturation as the wild type; instead, the K48A/L mutants were significantly destabilized, and aggregated above 65.0 °C (data not shown). As expected, T_m values determined by DSF showed a reduction of *ca.* 8.0 and 10.0 °C for K48A and K48L, respectively (Table 4). Thus, these data, consistently with the structural observations, demonstrated that the integrity of the *K48-network* contributes significantly to the protein stability; moreover, substitution of the E44 residue has minor impact on protein stability with respect to the K48 residue, in agreement with the central position and multiple intramolecular interactions established by this latter residue within the network in the free protein.

In conclusion, our biochemical analysis demonstrated that perturbation of the *K48-network* affects mainly *Ss*OGT stability, and at lesser extent its DNA repair activity, consistent with the notion that AGT alkylation has a minor effect on the DNA binding activity [10,39]. Taken together, these results support the hypothesis that the main role of the *K48-network* is contributing to stabilizing connection between the N_{ter} domain and the connecting loop.

4. Conclusions

Our combined structural, biochemical, mutational and molecular dynamics analysis demonstrate that the *K48-network*, along with the previously identified D27-R133 interaction, contributes to maintain the correct folding of *Ss*OGT and is perturbed after lesion recognition.

Based on our previous and present data, we propose a model of the conformational changes and fate of the *Ss*OGT upon the repair of alkylated DNA (Fig. 5). The optimal activity and stability of *Ss*OGT require coordination between the N_{ter} and C_{ter} domains of the protein; in fact, several intramolecular interactions are found at the interface

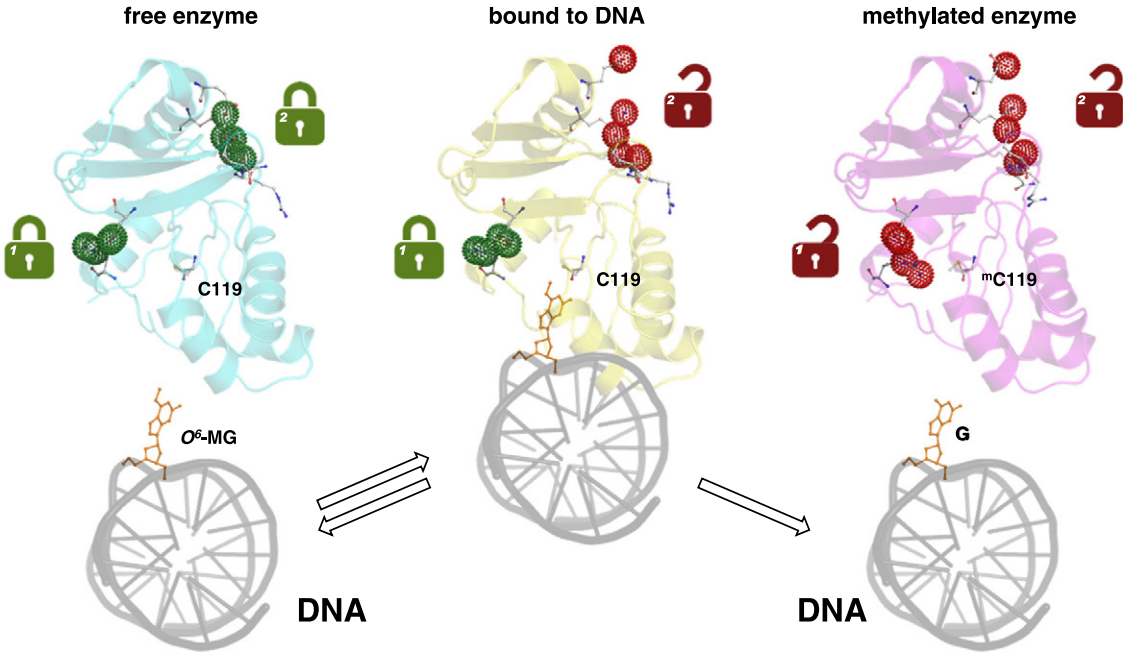

Fig. 5. Model of the conformational changes and fate of the SsOGT upon repair of alkylated DNA. The N_{ter} and C_{ter} domains of the free enzyme (*in cyan*; PDB ID: 4ZYE) are stabilized and coordinated by the presence of two *locks* (coloured dots), namely the D27-R133 interaction [10] and the *K48-network*, respectively. *Ss*OGT binds the DNA (*in yellow*, and *in gray*, respectively; PDB ID: 4ZYD) and recognizes the damaged guanine (O^6-MG, in orange *ball and stick* format), led to the opening only of the *lock 2*: this state could still allow the enzyme to dissociate the DNA and restore the *K48-network*. Upon the alkylation of the catalytic cysteine (^{m}C119), both the *locks* change to the open state, causing the irreversible conformational changes in charge of the alkylated-enzyme (*in magenta*; PDB ID: 4ZYG), and subsequently its destabilization. All the important residues for the activity of *Ss*OGT are drawn as *ball and stick*, and coloured as described in Fig. 1.

between the two domains, which are likely to contribute to interdomain communication. Our previous [10] and present work identified two groups of interactions, namely the D27-R133 pair and the *K48-network*, respectively, playing important role in protein stability, as well as in communicating the state of active site. We suggest that these interactions act as "*locks*": in the ligand-free protein, both *locks* are in their "closed state", thus ensuring the correct folding of the protein for its optimal stability and ready to perform the reaction. Binding to DNA and recognition of the damaged guanine lead to opening of *lock 2* only (through perturbation of the *K48-network*), destabilizing the link between the N_{ter} domain and the connecting loop. We hypothesize that this modification is reversible as long as the active site remains unmodified: if the protein dissociates from DNA without performing the repair reaction, the integrity of the *K48-network* is restored and the structural stability of the protein is preserved (Fig. 5). However, once the DNA repair reaction is completed, alkylation of the catalytic cysteine induces irreversible conformational changes, fixing the *lock 1* (formed by the D27-K133 ion pair) in its "open state" (Fig. 5). The loss of coordination between the N_{ter} and C_{ter} domains triggers the *Ss*OGT destabilization and, subsequently, its degradation.

To the best of our knowledge our studies provided the most detailed description of alkylation-induced conformational changes occurring in a protein of this class. The unavailability of a similarly detailed analysis for the human as well as other AGTs impairs extensive comparison of these results. By analysing the available structures of human AGT [7,13,19] we notice that the region corresponding to that containing the *K48-network* in *Ss*OGT, is characterized by the presence of hydrophobic residues that stabilize contacts between the α-helix belonging to the N-terminal domain and the random coiled loop connecting the two protein domains. Although this hypothesis could not be tested directly, due to the instability of alkylated hAGT structures, these hydrophobic interactions might play a role similar to the *Ss*OGT *K48-network*. Thus, our model might be extended to other AGTs, assuming that, whatever their nature, interdomain communication and coordination play a key role in maintaining proper folding and respond to alkylation triggering destabilization and degradation.

Supplementary data to this article can be found online at http://dx.doi.org/10.1016/j.bbagen.2016.10.020.

Transparency document

The Transparency document associated with this article can be found, in the online version.

Acknowledgments

We gratefully thank Dr. Andrea Strazzulli for assistance in some experiments. This work was supported by: FIRB-Futuro in RicercaRBFR12OO1G_002-Nematic.

References

[1] A.E. Pegg, Repair of O(6)-alkylguanine by alkyltransferases, Mutat. Res. 462 (2000) 83–100.
[2] A.E. Pegg, Multifaceted roles of alkyltransferase and related proteins in DNA repair, DNA damage, resistance to chemotherapy, and research tools, Chem. Res. Toxicol. 24 (2011) 618–639.
[3] A. Vettone, G. Perugino, M. Rossi, A. Valenti, M. Ciaramella, Genome stability: recent insights in the topoisomerase reverse gyrase and thermophilic DNA alkyltransferase, Extremophiles: life under extreme conditions 18 (2014) 895–904.
[4] R. Miggiano, V. Casazza, S. Garavaglia, M. Ciaramella, G. Perugino, M. Rizzi, F. Rossi, Biochemical and structural studies of the *Mycobacterium tuberculosis* O^6-methylguanine methyltransferase and mutated variants, J. Bacteriol. 195 (2013) 2728–2736.
[5] R. Miggiano, G. Perugino, M. Ciaramella, M. Serpe, D. Rejman, O. Pav, R. Pohl, S. Garavaglia, S. Lahiri, M. Rizzi, F. Rossi, Crystal structure of Mycobacterium tuberculosis O^6-methylguanine-DNA methyltransferase protein clusters assembled on to damaged DNA, Biochem. J. 473 (2016) 123–133.
[6] D.S. Daniels, J.A. Tainer, Conserved structural motifs governing the stoichiometric repair of alkylated DNA by O(6)-alkylguanine-DNA alkyltransferase, Mutat. Res. 460 (2000) 151–163.
[7] D.S. Daniels, T.T. Woo, K.X. Luu, D.M. Noll, N.D. Clarke, A.E. Pegg, J.A. Tainer, DNA binding and nucleotide flipping by the human DNA repair protein AGT, Nat. Struct. Mol. Biol. 11 (2004) 714–720.
[8] E.M. Duguid, P.A. Rice, C. He, The structure of the human AGT protein bound to DNA and its implications for damage detection, J. Mol. Biol. 350 (2005) 657–666.
[9] M.H. Moore, J.M. Gulbis, E.J. Dodson, B. Demple, P.C. Moody, Crystal structure of a suicidal DNA repair protein: the Ada O^6-methylguanine-DNA methyltransferase from *E. coli*, EMBO J. 13 (1994) 1495–1501.
[10] G. Perugino, R. Miggiano, M. Serpe, A. Vettone, A. Valenti, S. Lahiri, F. Rossi, M. Rossi, M. Rizzi, M. Ciaramella, Structure-function relationships governing activity and stability of a DNA alkylation damage repair thermostable protein, Nucleic Acids Res. 43 (2015) 8801–8816.
[11] G. Perugino, A. Vettone, G. Illiano, A. Valenti, M.C. Ferrara, M. Rossi, M. Ciaramella, Activity and regulation of archaeal DNA alkyltransferase: conserved protein involved in repair of DNA alkylation damage, J. Biol. Chem. 287 (2012) 4222–4231.
[12] J.L. Tubbs, A.E. Pegg, J.A. Tainer, DNA binding, nucleotide flipping, and the helix-turn-helix motif in base repair by O^6-alkylguanine-DNA alkyltransferase and its implications for cancer chemotherapy, DNA Repair 6 (2007) 1100–1115.
[13] J.E. Wibley, A.E. Pegg, P.C. Moody, Crystal structure of the human O^6-alkylguanine-DNA alkyltransferase, Nucleic Acids Res. 28 (2000) 393–401.
[14] Q. Fang, S. Kanugula, A.E. Pegg, Function of domains of human O^6-alkylguanine-DNA alkyltransferase, Biochemistry 44 (2005) 15396–15405.
[15] J.J. Rasimas, P.A. Dalessio, I.J. Ropson, A.E. Pegg, M.G. Fried, Active-site alkylation destabilizes human O^6-alkylguanine DNA alkyltransferase, Protein science: a publication of the Protein Society 13 (2004) 301–305.
[16] M. Xu-Welliver, A.E. Pegg, Degradation of the alkylated form of the DNA repair protein, O^6-alkylguanine-DNA alkyltransferase, Carcinogenesis 23 (2002) 823–830.
[17] S. Philip, S. Swaminathan, S.G. Kuznetsov, S. Kanugula, K. Biswas, S. Chang, N.A. Loktionova, D.C. Haines, P. Kaldis, A.E. Pegg, S.K. Sharan, Degradation of BRCA2 in alkyltransferase-mediated DNA repair and its clinical implications, Cancer Res. 68 (2008) 9973–9981.
[18] E. Brunk, B. Mollwitz, U. Rothlisberger, Mechanism to trigger unfolding in O^6-alkylguanine-DNA alkyltransferase, Chembiochem. Eur. J. Chem. Biol. 14 (2013) 703–710.
[19] D.S. Daniels, C.D. Mol, A.S. Arvai, S. Kanugula, A.E. Pegg, J.A. Tainer, Active and alkylated human AGT structures: a novel zinc site, inhibitor and extrahelical base binding, EMBO J. 19 (2000) 1719–1730.
[20] S. Kanugula, K. Goodtzova, A.E. Pegg, Probing of conformational changes in human O^6-alkylguanine-DNA alkyl transferase protein in its alkylated and DNA-bound states by limited proteolysis, Biochem. J. 329 (Pt 3) (1998) 545–550.
[21] G. Perugino, A. Valenti, A. D'Amaro, M. Rossi, M. Ciaramella, Reverse gyrase and genome stability in hyperthermophilic organisms, Biochem. Soc. Trans. 37 (2009) 69–73.
[22] A. Valenti, A. Napoli, M.C. Ferrara, M. Nadal, M. Rossi, M. Ciaramella, Selective degradation of reverse gyrase and DNA fragmentation induced by alkylating agent in the archaeon *Sulfolobus solfataricus*, Nucleic Acids Res. 34 (2006) 2098–2108.
[23] A. Valenti, G. Perugino, T. Nohmi, M. Rossi, M. Ciaramella, Inhibition of translesion DNA polymerase by archaeal reverse gyrase, Nucleic Acids Res. 37 (2009) 4287–4295.
[24] V. Visone, A. Vettone, M. Serpe, A. Valenti, G. Perugino, M. Rossi, M. Ciaramella, Chromatin structure and dynamics in hot environments: architectural proteins and DNA topoisomerases of thermophilic archaea, Int. J. Mol. Sci. 15 (2014) 17162–17187.
[25] A. Vettone, M. Serpe, A. Hidalgo, J. Berenguer, G. del Monaco, A. Valenti, M. Rossi, M. Ciaramella, G. Perugino, A novel thermostable protein-tag: optimization of the *Sulfolobus solfataricus* DNA-alkyl-transferase by protein engineering, Extremophiles: life under extreme conditions 20 (2016) 1–13.
[26] A. Gautier, A. Juillerat, C. Heinis, I.R. Correa Jr., M. Kindermann, F. Beaufils, K. Johnsson, An engineered protein tag for multiprotein labeling in living cells, Chem. Biol. 15 (2008) 128–136.
[27] Y. Cheng, W.H. Prusoff, Relationship between the inhibition constant (K1) and the concentration of inhibitor which causes 50 per cent inhibition (I50) of an enzymatic reaction, Biochem. Pharmacol. 22 (1973) 3099–3108.
[28] F.H. Niesen, H. Berglund, M. Vedadi, The use of differential scanning fluorimetry to detect ligand interactions that promote protein stability, Nat. Protoc. 2 (2007) 2212–2221.
[29] T.G. Battye, L. Kontogiannis, O. Johnson, H.R. Powell, A.G. Leslie, iMOSFLM: a new graphical interface for diffraction-image processing with MOSFLM, Acta Crystallogr. Sect. D: Biol. Crystallogr. 67 (2011) 271–281.
[30] M.D. Winn, C.C. Ballard, K.D. Cowtan, E.J. Dodson, P. Emsley, P.R. Evans, R.M. Keegan, E.B. Krissinel, A.G. Leslie, A. McCoy, S.J. McNicholas, G.N. Murshudov, N.S. Pannu, E.A. Potterton, H.R. Powell, R.J. Read, A. Vagin, K.S. Wilson, Overview of the CCP4 suite and current developments, Acta Crystallogr. Sect. D: Biol. Crystallogr. 67 (2011) 235–242.
[31] A.J. McCoy, R.W. Grosse-Kunstleve, P.D. Adams, M.D. Winn, L.C. Storoni, R.J. Read, Phaser crystallographic software, J. Appl. Crystallogr. 40 (2007) 658–674.
[32] P.D. Adams, P.V. Afonine, G. Bunkoczi, V.B. Chen, I.W. Davis, N. Echols, J.J. Headd, L.W. Hung, G.J. Kapral, R.W. Grosse-Kunstleve, A.J. McCoy, N.W. Moriarty, R. Oeffner, R.J. Read, D.C. Richardson, J.S. Richardson, T.C. Terwilliger, P.H. Zwart, PHENIX: a comprehensive Python-based system for macromolecular structure solution, Acta Crystallogr. Sect. D: Biol. Crystallogr. 66 (2010) 213–221.
[33] T.C. Terwilliger, R.W. Grosse-Kunstleve, P.V. Afonine, N.W. Moriarty, P.H. Zwart, L.W. Hung, R.J. Read, P.D. Adams, Iterative model building, structure refinement and density modification with the PHENIX AutoBuild wizard, Acta Crystallogr. Sect. D: Biol. Crystallogr. 64 (2008) 61–69.

[34] P. Emsley, B. Lohkamp, W.G. Scott, K. Cowtan, Features and development of Coot, Acta Crystallogr. Sect. D: Biol. Crystallogr. 66 (2010) 486–501.
[35] H.J.C. Berendsen, J.P.M. Postma, W.F. van Gunsteren, J. Hermans, Interaction models for water in relation to protein hydration, in: B. Pullman (Ed.), Intermolecular Forces: Proceedings of the Fourteenth Jerusalem Symposium on Quantum Chemistry and Biochemistry Held in Jerusalem, Israel, April 13–16, 1981, Springer Netherlands, Dordrecht 1981, pp. 331–342.
[36] H. Hashimoto, T. Inoue, M. Nishioka, S. Fujiwara, M. Takagi, T. Imanaka, Y. Kai, Hyperthermostable protein structure maintained by intra and inter-helix ion-pairs in archaeal O^6-methylguanine-DNA methyltransferase, J. Mol. Biol. 292 (1999) 707–716.
[37] H. Hashimoto, M. Nishioka, T. Inoue, S. Fujiwara, M. Takagi, T. Imanaka, Y. Kai, Crystallization and preliminary X-ray crystallographic analysis of archaeal O^6-methylguanine-DNA methyltransferase, Acta Crystallogr. Sect. D: Biol. Crystallogr. 54 (1998) 1395–1396.
[38] A. Roberts, J.G. Pelton, D.E. Wemmer, Structural studies of MJ1529, an O^6-methylguanine-DNA methyltransferase, Magnetic Resonance in Chemistry: MRC, 44 Spec No 2006, pp. S71–S82.
[39] J.J. Rasimas, A.E. Pegg, M.G. Fried, DNA-binding mechanism of O^6-alkylguanine DNA alkyltransferase. Effects of protein and DNA alkylation on complex stability, J. Biol. Chem. 278 (2003) 7973–7980.